

# RF-Molecular Beam Epitaxy Growth and Properties of InN and Related Alloys

Yasushi NANISHI, Yoshiki SAITO and Tomohiro YAMAGUCHI

The fundamental band gap of InN has been thought to be about 1.9 eV for a long time. Recent developments of metalorganic vapor phase epitaxy (MOVPE) and RF-molecular beam epitaxy (RF-MBE) growth technologies have made it possible to obtain high-quality InN films. A lot of experimental results have been presented very recently, suggesting that the true band-gap energy of InN should be less than 1.0 eV. In this paper, we review the results of the detailed study of RF-MBE growth conditions for obtaining high-quality InN films. The full widths at half maximum (FWHMs) of  $\omega$ -mode X-ray diffraction (XRD),  $\omega$ - $2\theta$  mode XRD and  $E_2$  (high-frequency)-phonon-mode peaks in the Raman scattering spectrum of the grown layer were 236.7 arcsec, 28.9 arcsec and  $3.7 \text{ cm}^{-1}$ , respectively. The carrier concentration and room temperature electron mobility were  $4.9 \times 10^{18} \text{ cm}^{-3}$  and  $1130 \text{ cm}^2/\text{Vs}$ , respectively. Photoluminescence and optical absorption measurements of these high-quality InN films have clearly demonstrated that the fundamental band gap of InN is about 0.8 eV. Studies on the growth and characterization of InGaN alloys over the entire alloy composition further supported that the fundamental band gap of InN is about 0.8 eV.

**KEYWORDS:** InN, InGaN, band gap, RF-MBE, characterization, PL, optical absorption, XRD, EXAFS, Raman scattering

## 1. Introduction

InN is a very attractive material for future optical and electronic devices. This is because of its outstanding material properties such as smallest effective mass, largest mobility, highest peak and saturation velocities, and smallest direct band gap in nitride semiconductors. However, until now, InN has been the least studied of nitride semiconductors. This is mainly due to the difficulty in obtaining high-quality InN crystals, which is due to the low dissociation temperature, high equilibrium vapor pressure of nitrogen molecules and the lack of suitable substrates for InN.

Studies on InN started in the beginning of the 20th century with an attempt to grow bulk InN from a melt.<sup>1)</sup> The attempt was not successful because of the low dissociation temperature and high vapor pressure of nitrogen molecules.<sup>2)</sup>

The next step in growing InN moved beyond the equilibrium approach to the non-equilibrium approach using various substrate materials by various growth methods including DC, RF, and magnetron sputtering.<sup>3-5)</sup> The InN films obtained by these methods in the 1970s and 1980s were all polycrystalline, some with an aligned orientation along the c-axis; the films also contained an extremely high defect density.

The physical parameters of InN were determined using these crystals. The first estimated direct band gap was about 1.9 eV.<sup>6)</sup> However, other studies reported values ranging from 1.7 to 3.1 eV.<sup>3,7-11)</sup> The most commonly cited measurement on optical absorption is that of Tansley and Foley;<sup>12)</sup> they reported band gap energy of 1.89 eV at room temperature.

In the late 1980s, improvements in growth techniques have made it possible to obtain single-crystalline InN. Single-crystalline InN was reported by Matsuoka *et al.*<sup>13)</sup> for the

first time in 1989 using metalorganic vapor phase epitaxy (MOVPE). Subsequently, several efforts<sup>14,15)</sup> were made to improve the quality of InN and high-quality films with carrier concentrations on the order of  $10^{18} \text{ cm}^{-3}$  and mobilities of  $730 \text{ cm}^2/\text{Vs}$ <sup>16)</sup> were obtained. Growth by MOVPE, however, has an inherent disadvantage because it must satisfy the conditions for  $\text{NH}_3$  pyrolysis and InN dissociation, which impose conflicting temperature requirements.

In contrast, molecular beam epitaxy (MBE) equipped with an RF plasma source has an essential advantage over MOVPE for obtaining high-quality InN. In this growth method, neutral and ionized excited-state nitrogen atoms and molecules can be generated separately by plasma sources. Thus, the crystal growth temperature can be set independently without considering the nitrogen source.

The first attempt to grow single-crystalline InN by the RF-MBE method was reported by Hoke *et al.* in 1991.<sup>17)</sup> Improvements in crystal quality were realized by various techniques such as insertion of low-temperature GaN,<sup>18)</sup> AlN,<sup>19)</sup> and InN<sup>20)</sup> buffer layers. Within a relatively short period of time, MBE growth studies produced high-quality films with residual electron concentrations of  $1.6 \times 10^{18} \text{ cm}^{-3}$  and a room temperature mobility of  $1180 \text{ cm}^2/\text{Vs}$ .<sup>18)</sup> Such rapid progress is probably due to the inherent advantage of the MBE growth method.

Photoluminescence (PL) and optical absorption were used to study single-crystalline InN films that were grown using MOVPE and MBE. These studies revealed that the fundamental band gap of single-crystalline InN was about 0.8 eV<sup>21-25)</sup> instead of 1.9 eV, determined by optical absorption using polycrystalline InN.

In this paper, we review the detailed studies of InN and InGaN growth by RF-MBE.

First, fundamental studies on basic growth processes are reviewed; these include the initial growth stage, two-step growth processes, the precise control of V/III ratio, and the resultant crystal properties of the grown films. Then we describe how precise control of growth temperature and insertion of low-temperature intermediate layers can be used to grow higher-quality InN films. Our group used a wide variety of techniques to determine the crystallographic, electrical, and optical properties of high-quality InN films. The techniques include X-ray diffraction (XRD), *in situ* reflection high-energy electron diffraction (RHEED), extended X-ray absorption fine structure (EXAFS), Rutherford backscattering (RBS), atomic force microscopy (AFM), coaxial impact-collision ion scattering spectroscopy (CAICISS), Hall effect measurements, PL, cathode-luminescence (CL), optical absorption, photo modulated reflectance, infrared spectroscopic ellipsometry, and Raman scattering. Typical results are described in §4.

Finally, InGaN films were grown over the entire range of alloy composition on sapphire substrates by inserting InN buffer layers. Results on optical absorption, CL, and PL measurements are presented.

## 2. Fundamental Study of Growth Process

### 2.1 Growth system and standard growth conditions

The growth of InN by RF-MBE was carried out in an MBE growth chamber equipped with a high-speed turbo-molecular pump (1500 liter/s) that evacuated the chamber up to  $1 \times 10^{-10}$  Torr. This MBE system is also equipped with a SVTA radical cell (model 2.75) to serve as the nitrogen source. The substrates used were mainly (0001) sapphire substrates. The back surface was coated with a

**Table I.** Lattice mismatch values of III-N semiconductors and sapphire substrates.

|     | $[11\bar{2}0]_{\text{III-N}} \parallel [11\bar{2}0]_{\text{sapphire}}$ | $[10\bar{1}0]_{\text{III-N}} \parallel [11\bar{2}0]_{\text{sapphire}}$ |
|-----|--|--|
| AlN | -34.6%   | +13.3%   |
| GaN | -33.0%   | +16.0%   |
| InN | -25.4%   | +29.2%   |

1- $\mu\text{m}$ -thick layer of molybdenum. They were set on an In-free molybdenum holder after being cleaned with organic solvents. High-purity (6N) In and Ga were used as group III materials and were evaporated from standard effusion cells. High-purity  $\text{N}_2$  gas (6N) was supplied to the RF plasma cell after passing through a Saes Getter purifier (model Monotorr Phase II 3000) to eliminate impurities including  $\text{H}_2\text{O}$ ,  $\text{H}_2$ ,  $\text{O}_2$ ,  $\text{CO}$ , and  $\text{CO}_2$  gases. Nitrogen gas of 2 sccm, which produced a pressure of  $1 \times 10^{-4}$  Torr, was supplied for InN growth. The typical growth rate of InN was approximately 500 nm/h. Growth temperatures were carefully monitored with a pyrometer at each growth run.

### 2.2 Initial growth stage

In contrast to GaN and AlN that grow on sapphire substrates with their *a*-axis orientation rotated  $30^\circ$  to become  $[10\bar{1}0]_{\text{GaN,AlN}} \parallel [11\bar{2}0]_{\text{sapphire}}$ , InN tends to grow with both  $[10\bar{1}0]_{\text{InN}} \parallel [11\bar{2}0]_{\text{sapphire}}$  and  $[11\bar{2}0]_{\text{InN}} \parallel [11\bar{2}0]_{\text{sapphire}}$  and easily form polycrystals.<sup>26)</sup> This is due to the fact that lattice mismatch

values of these two cases are very close, which is not the case for GaN and AlN, where lattice mismatch is much smaller when the *a*-axis rotates by  $30^\circ$  to become  $[10\bar{1}0]_{\text{GaN,AlN}} \parallel [11\bar{2}0]_{\text{sapphire}}$ . The lattice mismatch values of nitride semiconductors and sapphire substrates for these two cases are compared in Table I.

Figure 1 shows the X-ray diffraction (XRD) pole figure of InN measured using asymmetric  $\{10\bar{1}2\}$  reflection. The InN film was grown at  $550^\circ\text{C}$  directly on a (0001) sapphire substrate without nitridation. This InN film has three domains: (A) the main domain with  $[10\bar{1}0]_{\text{InN}} \parallel [11\bar{2}0]_{\text{sapphire}}$ , (B) the domain with  $[11\bar{2}0]_{\text{InN}} \parallel [11\bar{2}0]_{\text{sapphire}}$ , and (C) another domain rotated by approximately  $19^\circ$  in the opposite direction from the main domain. The detailed atomic arrangements for these three cases are shown in ref. 27.

The ratio of domain (A) to domain (B) is very sensitive to growth temperature. Domain (A) is dominant when the films are grown at higher temperatures ( $540^\circ\text{C}$ ). Domain (B) is dominant when they are grown at lower

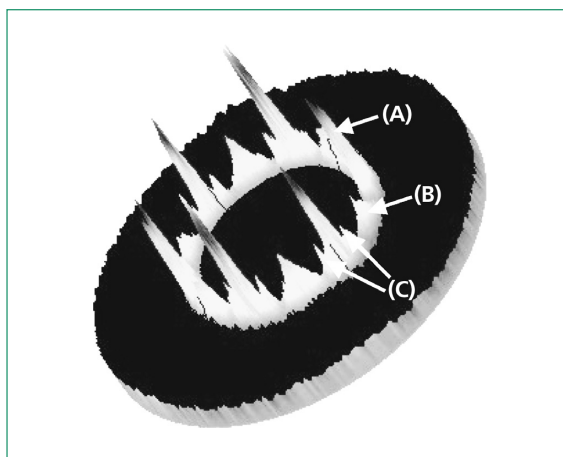
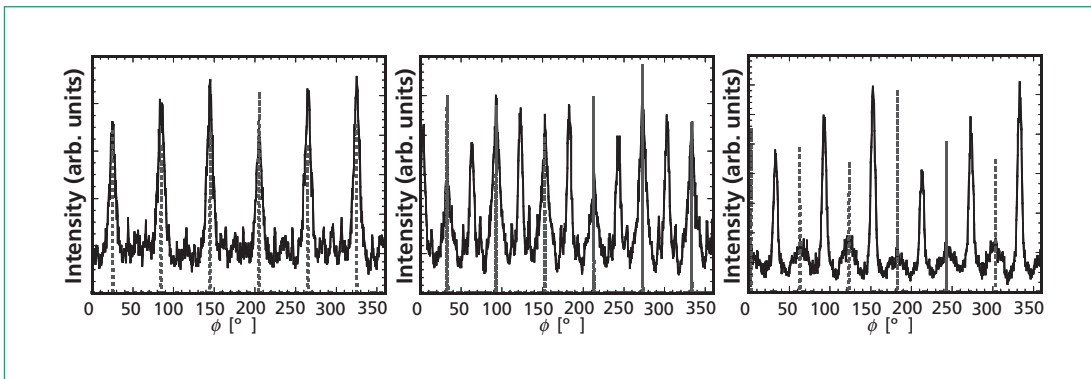


**Fig.1.** X-ray diffraction (XRD) pole figure of the InN grown directly at  $550^\circ\text{C}$ . Asymmetric InN  $\{10\bar{1}2\}$  reflections are used.

Fig.2. XRD  $\phi$  scan measurement for InN grown with growth temperatures of (a) 520°C, (b) 530°C and (c) 540°C. The solid line shows the peaks for the asymmetric InN {1122} reflections, whereas the dotted line shows the peaks for the asymmetric sapphire {1123} reflections.



temperatures (520°C), as shown in Fig.2. A steeper transition from domain (A) to domain (B) occurs when the V/III ratio is low. This is probably due to the greater migration of In under these conditions.<sup>28,29)</sup> Thermodynamically stable conditions can be realized more easily if the V/III ratio is low, as can be easily produced in GaN RF-MBE growth experiments.

These results imply that InN tends to include a multidomain structure and form polycrystals if the optimum growth conditions such as growth temperature and V/III ratio are not carefully selected in the initial growth stage.<sup>28,29)</sup> The nitridation of the sapphire substrates prior to InN growth is a very effective way of determining the *a*-axis direction to  $[10\bar{1}0]_{\text{InN}} \parallel [11\bar{2}0]_{\text{sapphire}}$  at all growth temperatures (Fig.3). We assume that nitridation results in the formation of an AlN or AlON layer on the substrate. This layer has the  $[10\bar{1}0]_{\text{AlN}}$

$\parallel [11\bar{2}0]_{\text{sapphire}}$  orientation, which results in the  $[10\bar{1}0]_{\text{InN}} \parallel [10\bar{1}0]_{\text{AlN}} \parallel [11\bar{2}0]_{\text{sapphire}}$ -oriented film.<sup>27)</sup>

### 2.3 Two-step growth

To grow high-quality InN films, obtaining atomically flat surfaces is essential. The application of the two-step growth method, which involves low-temperature buffer growth at about 550°C prior to the main epitaxial growth at about 1000°C, is very effective for growing flat and high-quality GaN and Al-GaN films on sapphire substrates by MOVPE. Studies on the surface morphologies of InN MOVPE films, however, have indicated that flatter surfaces can be obtained when the growth temperature is higher. A reduction in the growth temperature to approximately 550°C makes the surface less flat.<sup>30)</sup> The growth of InN at temperatures below 500°C is effectively impossible for MOVPE because

of the limitation of the pyrolysis temperature of  $\text{NH}_3$  gas.

In this RF-MBE growth study, InN buffer layers of about 30 nm thick were grown at 300°C for 10 min and then annealed at 550°C.<sup>31)</sup> Figure 4 shows the RHEED patterns and surface morphologies of an InN buffer layer grown at 300°C (a) before and (b) after annealing at 550°C. This figure indicates that the surface morphology was improved by annealing at 550°C.

When the InN film is grown directly on the sapphire substrate at higher temperatures near 550°C, the film easily forms three-dimensional morphology, as shown in a typical cross-sectional SEM image in Fig.5.<sup>20)</sup>

The crystal quality of the buffer layer grown at 300°C is poor due to inadequate In migration on the surface. However, the crystallinity as well as surface flatness of the InN film was remarkably improved by consecutive

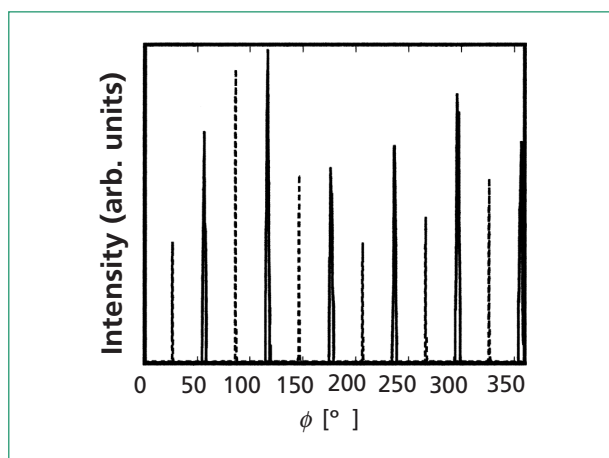


Fig.3. Result of  $\phi$  scan measurement of the InN film after the nitridation process. The solid line shows the peaks for the asymmetric InN {1122} reflections, whereas the dotted line shows the peaks for the asymmetric sapphire {1123} reflections.

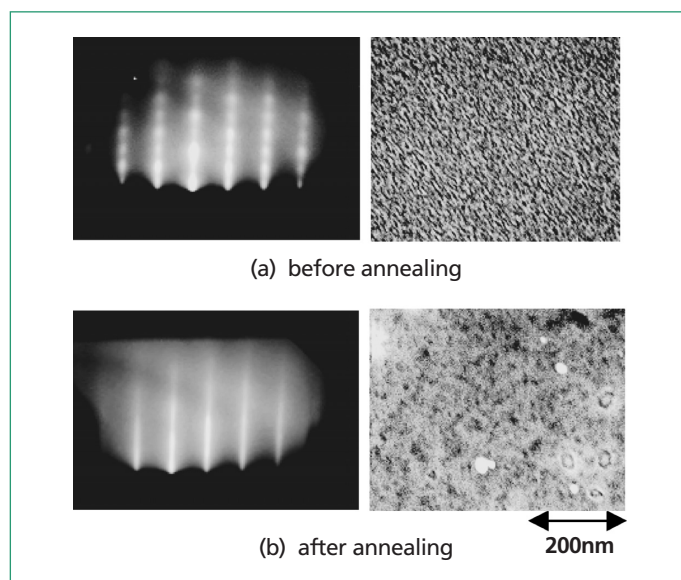


Fig.4. RHEED patterns ( $e \parallel [1120]$ ) and surface morphology obtained by SEM observation of InN buffer layer; (a) before and (b) after annealing at 550°C.

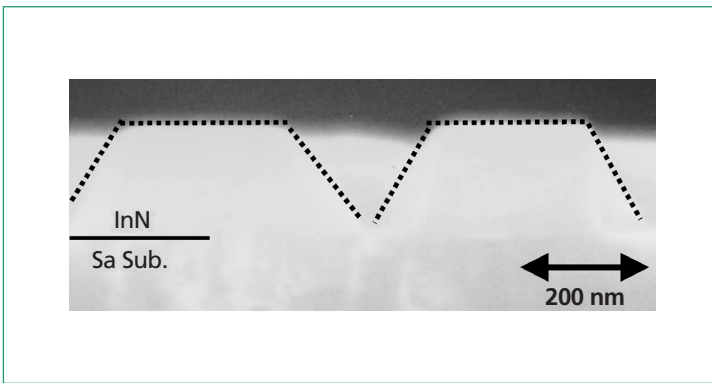


Fig.5. Cross-sectional SEM image of InN grown at 550°C.

annealing. Improvement in crystal quality is evident from the RBS results before and after annealing at 550°C. Figure 6 shows a comparison of RBS yield between (0001)-aligned and random directions from low-temperature-grown InN buffer layer without (a) and with (b) annealing at 550°C. The  $\chi_{\min}$  values of InN buffer layers with and without annealing were 14% and 66%, respectively. The quantity  $\chi_{\min}$  varies from near 0 for nearly perfect single crystals up to 100% for amorphous or polycrystalline materials. Based on these studies, the two-step growth temperature diagram shown in Fig.7 was fixed as the diagram for a standard growth process of RF-MBE.

#### 2.4 V/III ratio and crystal polarity

The control of V/III ratio is by far the most important issue to obtain high-quality InN by MBE. At temperatures below the dissociation temperature of InN (approximately 550°C), the vapor pressure of nitrogen molecules over InN is much higher than the In vapor pressure over In metal.<sup>32)</sup> To suppress the dissociation of InN films, one should have a nitrogen pressure higher than the equilibrium pressure during the entire growth process.

Once the beam equivalent pressure of In exceeds the equivalent nitrogen pressure from surface stoichiometry, In droplets should form on the surface. They cannot evaporate

from the surface at the selected growth temperature below the dissociation temperature. This implies that InN should be grown under N-rich conditions.

On the other hand, high-quality GaN can be grown under slightly Ga-rich conditions due to the enhanced migration of Ga. This should be the case also for InN growth by MBE, as was implied in the experiment presented in §2.2.

Considering all these limitations for InN MBE growth, V/III ratio should be controlled as close as possible to stoichiometry from the N-rich side. Also, to guarantee sufficient migration of In, the growth temperature should be set at the highest possible temperature without noticeable dissociation of the InN film. By keeping the growth temperature, beam equivalent pressure of In, and N<sub>2</sub> flow rate all constant at 550°C,  $3.2 \times 10^{-7}$  Torr, and 2.0 sccm, respectively, the effective V/III ratio on the growing surface was carefully controlled by changing the RF-plasma power between 230 and 250 W.

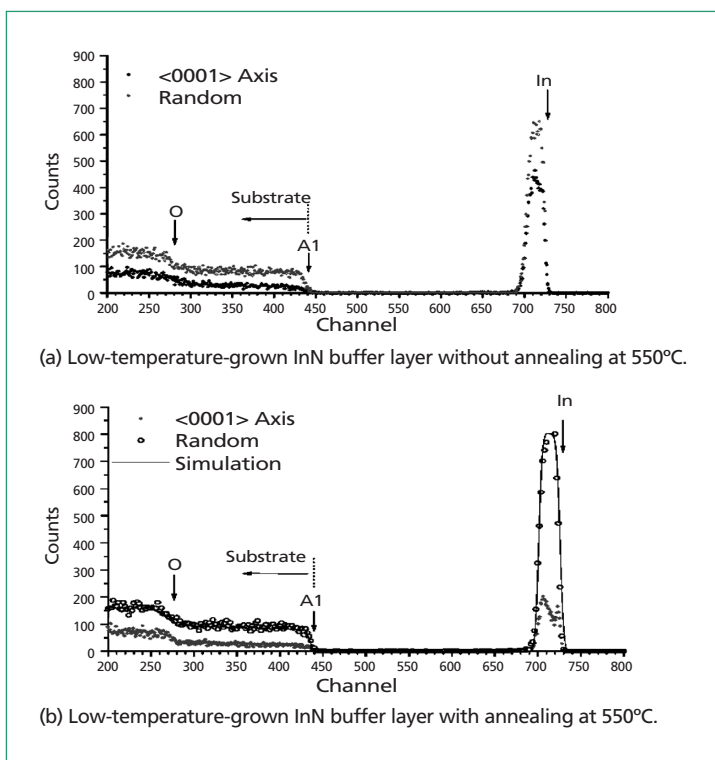


Fig.6. RBS results of low-temperature-grown InN buffer layers (a) without and (b) with annealing.

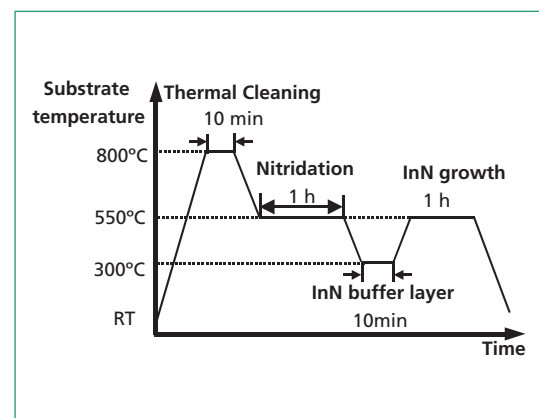


Fig.7. Two-step-growth temperature diagram.

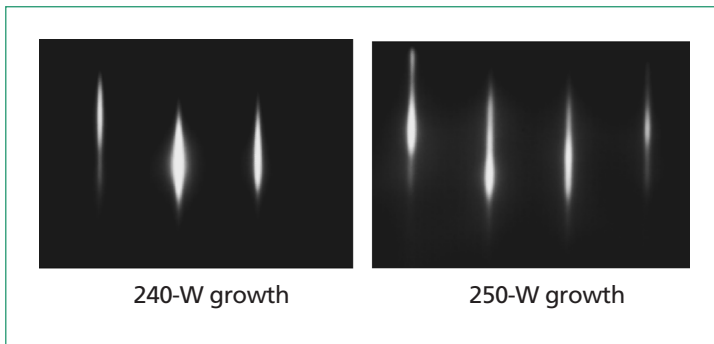


Fig.8. RHEED patterns of InN epilayer. (e || [1120]).

Figure 8 shows the RHEED patterns of the InN films grown for 1 h with RF-plasma powers of 240 and 250 W.<sup>33)</sup> These films are about 250 nm thick. The RHEED patterns have clear streaks, indicating that the InN surfaces are smooth at the atomic level. The root mean square (RMS) roughness characterized by AFM for these two surfaces of an area of  $1 \mu\text{m} \times 1 \mu\text{m}$  were 1.5 and 3.6 nm, respectively, which confirmed the excellent surface morphology of these two samples. The InN grown at an RF-plasma power of 230 W, however, did not show any RHEED patterns, due to its surface having many In droplets.

The cross-sectional SEM images of these InN films are shown in Fig.9.<sup>20)</sup> A high density of In droplets is observed for the sample grown under an RF-plasma power of 230 W, apparently due to a lack of an active nitrogen source. The pit size of the InN grown at 240 W is much smaller than that of the 250-W sample. Presumably, the 240-W sample was grown under a condition closer to surface stoichiometry, and the 250-W sample should have been grown under a deeper N-rich condition.

Figure 10 shows a comparison of the  $\omega$ - $2\theta$  scan XRD of InN between the 240-W and 250-W samples. Diffraction peaks corresponding to the (0002) and (0004) from Wurtzite InN and the (0006) diffraction peak from sapphire are observed for the 250-W sample. A very small peak corresponding to the In metal occurs in scan for the 240-W sample, which is probably due to the slightly In-rich condition.<sup>33)</sup> The full widths at half maximum (FWHMs) of the InN (0002) peak of these two samples were approximately 300 arcsec. Figure 11 shows a comparison of

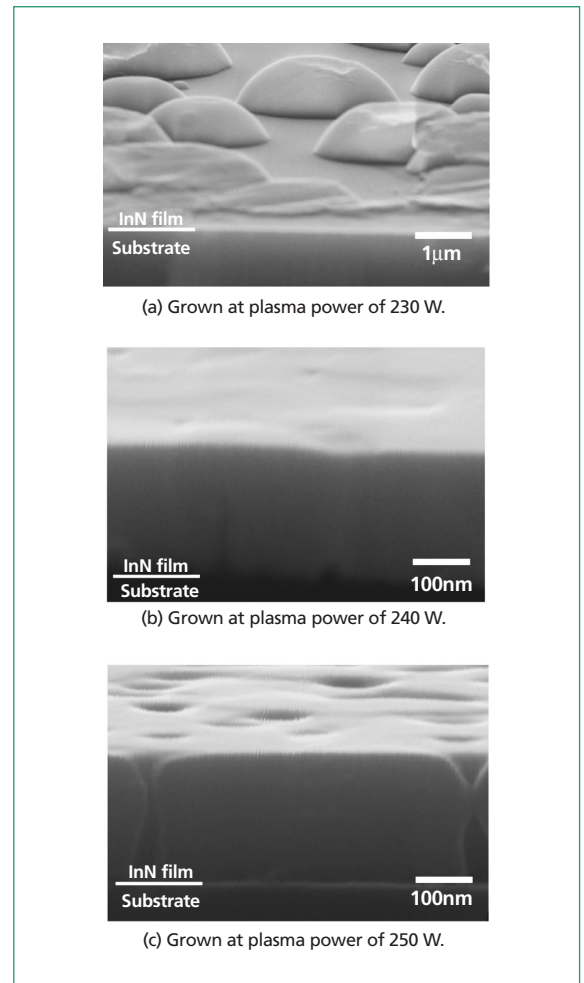


Fig.9. Surface morphology of InN grown at plasma powers of (a) 230 W, (b) 240 W and (c) 250 W.

the  $\omega$ -scan X-ray diffraction rocking curve of (0002) InN between the 240-W and 250-W samples. These two curves are similar in terms of their FWHM of 25 arcmin. The carrier density and room temperature mobility of these films were approximately  $3 \times 10^{19} \text{ cm}^{-3}$  and  $760 \text{ cm}^2/\text{Vs}$ , respectively. Thus, the precise control of V/III ratio is needed to obtain high-quality InN by RF-MBE.<sup>33)</sup>

The polarity of InN grown by RF-MBE was characterized by CAICISS and it was found that the polarity of InN is much more sensitive to growth temperature than that of other nitride semiconductors.<sup>34)</sup> N polarity was observed for the low-temperature growth of InN at 300°C, whereas the high-temperature growth of InN over 550°C primarily showed In polarity.<sup>34)</sup>

This result is consistent with that of a GaN decomposition experiment by an *in situ* gravimetric monitoring (GM) method using free-standing GaN (0001), in which the etch-

ing rate of the GaN (000 $\bar{1}$ ) surface is reported to be higher than that of the GaN (0001) surface at high temperatures. The relationship is opposite in the low-temperature region.<sup>35)</sup>

The above experimental results are explained as follows.<sup>35)</sup> The decomposition of GaN is limited by the Ga surface in the high-temperature region where each topmost Ga atom on the GaN (0001) surface combines with three N atoms (three back bonds) whereas Ga atom on the GaN (000 $\bar{1}$ ) surface each forms one back bond with only one N atom in the bulk. On the other hand, the limiting surface is the N surface in the low-temperature region. Thus the decomposition rate of GaN (0001) is faster than that of GaN (000 $\bar{1}$ ) because each N atom on the GaN (0001) surface combines with one Ga atom in the bulk (one back bond), whereas each N atom on GaN (000 $\bar{1}$ ) form back bonds to three Ga atoms in the bulk.<sup>35)</sup>

The condition of the InN surface in the

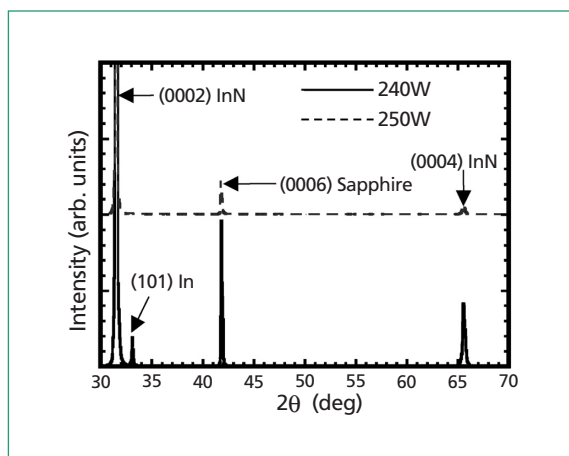


Fig. 10.  $\omega$ - $2\theta$  scan XRD curves for InN grown at plasma powers of 240 W and 250 W.

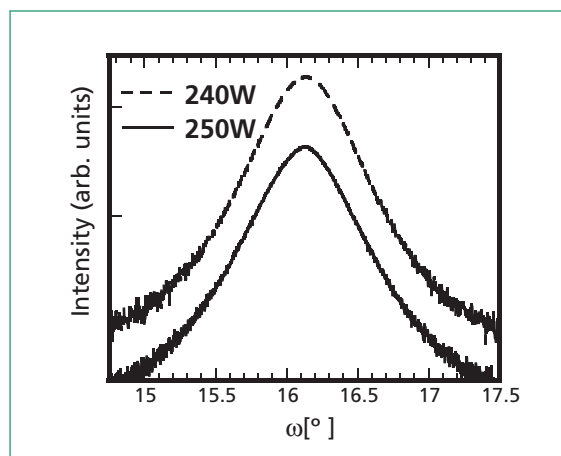


Fig. 11.  $\omega$ -scan XRC of (0002) InN grown at plasma powers of 240 W and 250 W.

etching mode should be the same as that of the GaN surface, and InN (0001) is thus more stable than InN (000 $\bar{1}$ ) at high temperatures. Also InN (000 $\bar{1}$ ) should become more stable than InN (0001) at low temperatures.

Considering the discussion of V/III ratio control and the polarity mentioned above, more stable growth is expected on InN (000 $\bar{1}$ ) surfaces, as InN growth should be carried out at low temperatures. The study of InN growth on the substrate with well-controlled polarity is under way and the result will be presented in a separate paper.

### 3. Improvement of Crystal Quality

#### 3.1 Growth temperature

We carefully controlled growth temperature and monitored the corresponding Raman scattering spectra to improve the crystalline

quality of InN. The Raman spectra obtained are shown in Fig. 12 for InN films grown at 550, 530, 520, 500, and 460°C. The theoretically expected  $E_2$  (high-frequency)-mode,  $E_2$  (low-frequency)-mode and  $A_1$  (LO)-mode are clearly observed at 491, 88, and 589  $\text{cm}^{-1}$ , respectively.<sup>25)</sup>

The peak positions and FWHM of dominant  $E_2$  (high-frequency)-phonon-mode peaks are summarized in Table II. The dependence of peak position on growth temperature may be due to the difference in residual stress between the films. An FWHM as narrow as 3.7  $\text{cm}^{-1}$  for the  $E_2$  (high-frequency)-phonon-mode peak was obtained for the film grown at 550°C. This FWHM is the narrowest value ever reported for InN films.<sup>25)</sup> These results indicate that the crystalline quality was improved by increasing the growth temperature within the dissociation limit of InN.

#### 3.2 Low temperature intermediate layer

The thickness of the layer grown by RF-MBE presented in §2.3 and §2.4 was about 250 nm. InN in and around the buffer layer on the sapphire substrate should contain a lot of defects and the electrical and optical properties in the region of defects are expected to be very poor.

To improve the overall quality of the InN films, thicker layers should be grown. The growth of thicker InN layers, however, is not easy because once In droplets are formed during growth, it is very difficult to remove them, thus one cannot achieve continuous stable growth.

We found that low-temperature-grown intermediate layers are very effective in obtaining thicker (>250 nm) and higher-quality InN layers. The details of this technique are given in ref. 36.

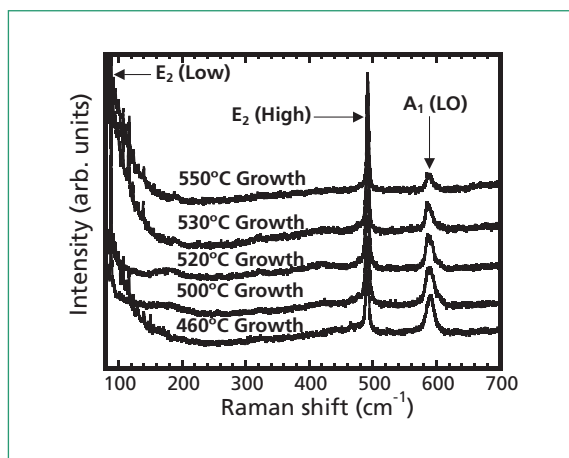


Fig. 12. Raman spectra for InN films grown at 550°C, 530°C, 520°C, 500°C and 460°C.

Table II. Peak positions and FWHM of dominant  $E_2$  (high)-phonon-mode peaks.

| Growth Temperature [°C] | $E_2$ (high) peak position [ $\text{cm}^{-1}$ ] | FWHM of $E_2$ (high) peak [ $\text{cm}^{-1}$ ] |
|-------------------------|---|--|
| 550                     | 491.9   | 3.7  |
| 530                     | 491.4   | 4.0  |
| 520                     | 491.2   | 4.4  |
| 500                     | 491.1   | 4.4  |
| 460                     | 491.2   | 4.1  |

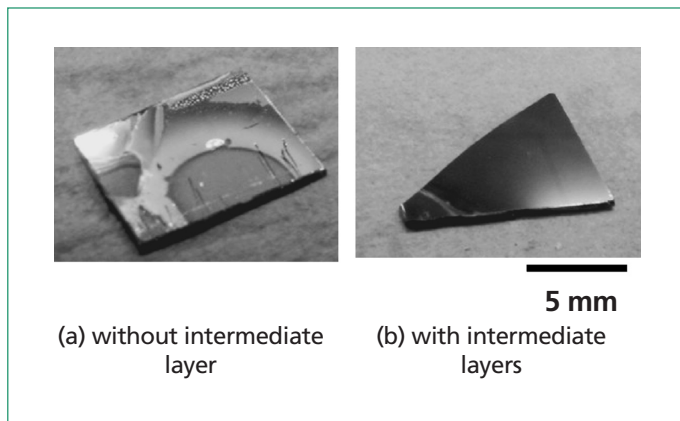


Fig.13. Optical microscopy images of InN grown (a) without and (b) with intermediate layers.

Figure 13 shows a comparison between optical microscope images of 600-nm thick InN layers grown with and without intermediate layers. Two intermediate layers 10 nm thick each were inserted into sample (B). The surface of this InN was mirror-smooth, whereas the surface of InN grown without an intermediate layer (A) has black and white areas. Here, areas with In droplets look white.

By growing films with thicknesses up to 1500 nm, we studied the dependence of electrical properties on film thickness. The results are shown in Fig.14. Much improvement in electrical properties is obtained with an increase in film thickness.

#### 4. Characterization

Here, we summarize the crystallographic, electrical, and optical properties of 1.5- $\mu\text{m}$ -thick InN layers. For crystallographic characterization, the  $\omega$ -scan X-ray diffraction rocking curve (XRC) and  $\omega$ - $2\theta$  scan XRD results were used. A typical XRC is shown in Fig.15. The FWHM of this curve is 236.7 arcsec. Fig-

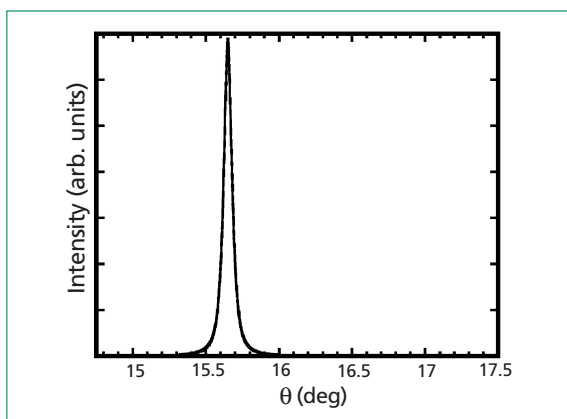


Fig.15.  $\omega$ -scan XRC of (0002) InN for the sample with film thickness of 1500 nm.

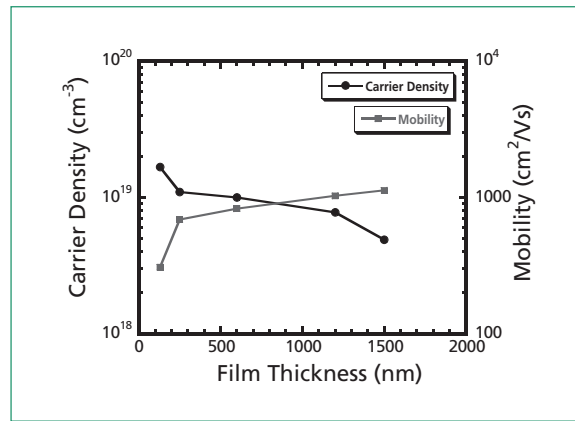


Fig.14. Dependence of electrical properties on film thickness.

ure 16 shows a typical  $\omega$ - $2\theta$  XRD curve, which gives a FWHM of only 28.9 arcsec, indicating an excellent crystallographic quality of the film.

The local atomic structure near In atoms was investigated using EXAFS oscillation of the In K edge.<sup>37)</sup> The signals from the first-nearest neighbor atoms (N) and second-nearest atoms (In) from In atoms were clearly observed. The atomic bond lengths of In-N and In-In were estimated to be  $d_{\text{In-N}}=0.215$  nm and  $d_{\text{In-In}}=0.353$  nm, respectively. The In-In bond length of 0.353 nm is close to the  $a$ -axis lattice constant of 0.3536 nm, which was calculated using XRD. Thus, the obtained local atomic structure agreed with the ideal structure of  $sp^3$  hybridization bonds.<sup>37)</sup>

A series of data obtained by Hall-effect measurement are summarized in Fig.17. Samples of various thicknesses grown under various conditions are also shown in this figure. The best 1.5- $\mu\text{m}$ -thick film obtained so far in this study has a carrier concentration of  $4.9 \times 10^{18} \text{ cm}^{-3}$  and a room temperature

mobility of  $1130 \text{ cm}^2/\text{Vs}$ . The source of this high-level residual carrier concentration, however, remains unclear.

The room-temperature PL spectra of a 250-nm-thick film grown with precisely controlled temperatures, as described in §3.1, are shown in Fig.18. Here,  $\text{Ar}^+$  laser at 514.5 nm with a power density of  $2.2 \text{ W}/\text{cm}^2$  was used as an excitation source. An InGaAs photodetector with a cutoff wavelength of  $2.05 \mu\text{m}$  was used. The wavelength of the PL peak position did not show any noticeable change even if the excitation power was changed over two orders of magnitude from  $65 \text{ mW}/\text{cm}^2$  to  $6.5 \text{ W}/\text{cm}^2$ .

The PL spectra at room temperature and 77 K observed for 1.5- $\mu\text{m}$ -thick InN are shown in Fig.19. Very strong and sharp luminescence was observed at 77 K with an FWHM of 24 meV. The FWHM at room temperature was 38 meV. This PL should originate from the fundamental interband transition of the InN film. No PL corresponding to 1.9 eV transition could be observed from any

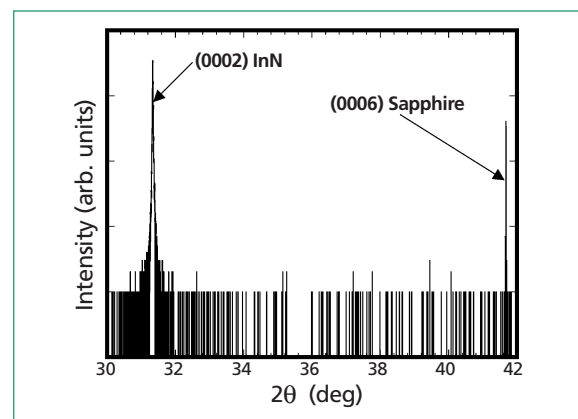


Fig.16.  $\omega$ - $2\theta$  XRD curve for InN sample with film thickness of 1500 nm.

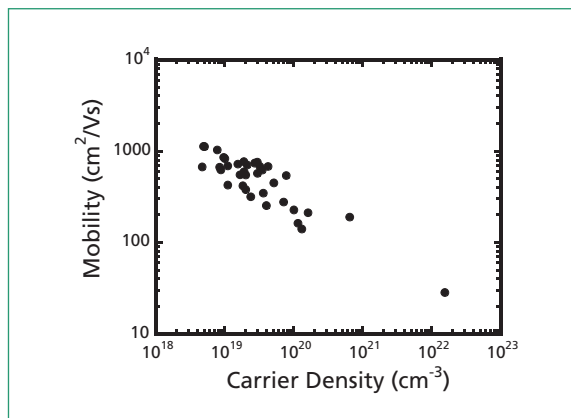


Fig.17. Electrical properties of InN films measured by Hall-effect measurements.

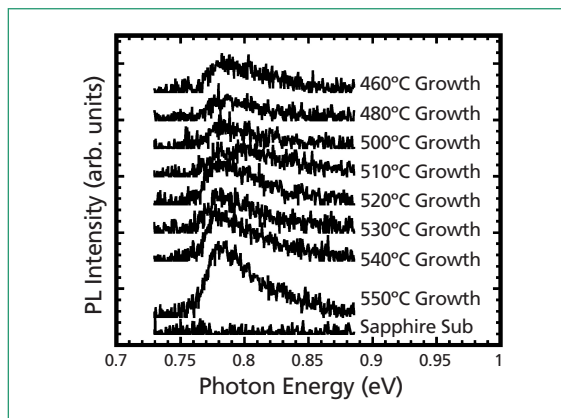


Fig.18. Room-temperature PL spectra of the InN film grown at 460–550°C.

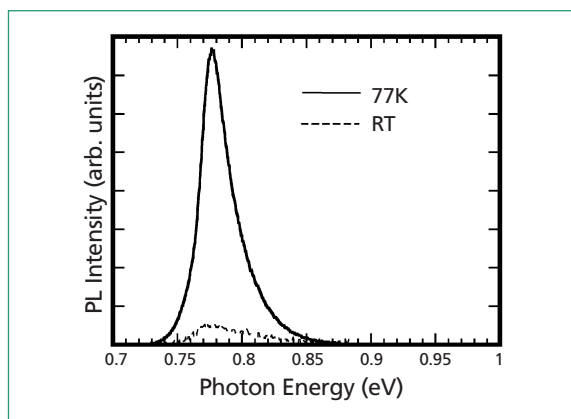


Fig.19. PL spectra both at room temperature and 77 K for relatively thick InN film.

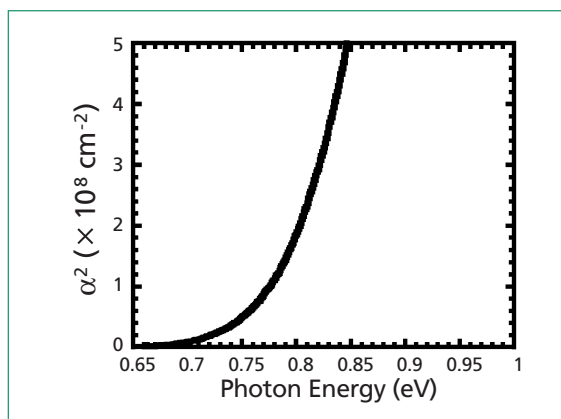


Fig.20. Room-temperature optical absorption coefficient squared of InN grown at 550°C versus the photon energy.

InN films grown in this study.

The optical absorption of InN grown at 550°C was also studied at room temperature. The optical absorption coefficient squared versus the photon energy is shown in Fig.20.

All of these results obtained by optical measurements suggest that the fundamental band gap of the high-quality single-crystalline InN grown by RF-MBE is approximately 0.8 eV at room temperature. This supports the most recent proposal<sup>[21–25]</sup> that the fundamental band gap is about 0.8 eV, which is much lower than the commonly accepted value of 1.9 eV.

The InN samples grown in this study were sent to UC Berkeley so that their optical properties could be characterized by optical absorption, PL, and photo-modulated reflectance techniques. The results were essentially the same as those presented in this paper.<sup>[24]</sup>

Measurements by infrared spectroscopic ellipsometry and micro-Raman scattering were also used to study the vibrational and electronic properties of the high-quality InN obtained in the study. Combining the results

of the ellipsometry data analysis with those of the Hall-effect measurement, the isotropically averaged effective electron mass in InN is 0.14  $m_0$ .<sup>[38]</sup>

## 5. InGaN Growth and Characterization

InGaN films with the entire alloy composition were grown on (0001) sapphire substrates at 550°C by RF-MBE after a low-temperature buffer layer was grown at 280°C.

The In beam flux was varied from  $1.0 \times 10^{-8}$  to  $4.0 \times 10^{-8}$  Torr so that the In composition of InGaN could be adjusted between  $x=0$  (for GaN) and  $x=1$  (for InN).<sup>[39]</sup>

The solid composition of the grown layer was determined by XRD. Here, all the layers are assumed to be fully relaxed. The solid composition versus In beam ratio (In flux to total flux ratio) is plotted in Fig.21. Unlike in the case of MOVPE, the solid composition was simply determined by the In-to-Ga

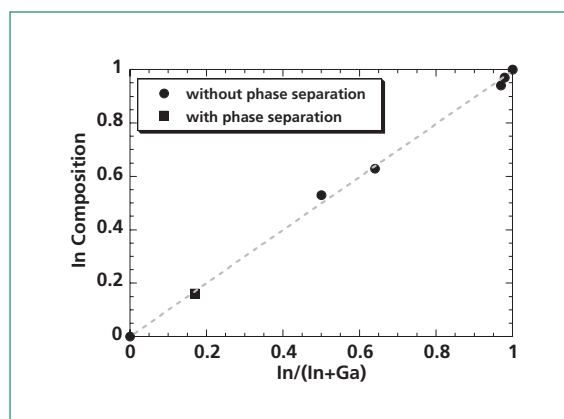


Fig.21. Solid composition versus In beam flux-to-total flux ratio. Solid composition of the grown layer was determined by XRD. Samples shown by ● have not phase separation in  $\omega$ -2 $\theta$  XRD, whereas sample shown by ■ has a slight phase separation in  $\omega$ -2 $\theta$  XRD.

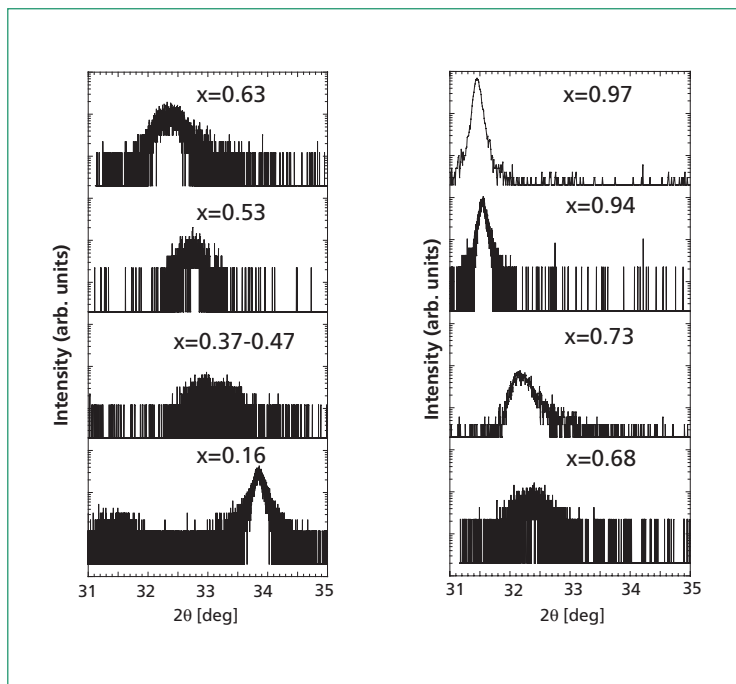


Fig.22.  $\omega$ - $2\theta$  XRD curves for  $\text{In}_x\text{Ga}_{1-x}\text{N}$  ( $x=0.16, 0.37-0.47, 0.53, 0.63, 0.68, 0.73, 0.94, 0.97$ ).

flux ratio. A large difference between solid composition and vapor phase composition were reported when high-quality InGaN layers were grown at 800°C by MOVPE.<sup>40)</sup> All the InGaN layers with various solid compositions grown at 550°C in this study have sufficiently good crystalline quality to emit strong PL at 77 K, which will be shown later in this section. The easy control of InGaN solid composition is another advantage of the RF-MBE growth method.

Figure 22 shows the  $\omega$ - $2\theta$  XRD curves for  $\text{In}_x\text{Ga}_{1-x}\text{N}$  ( $0 < x < 1$ ). We confirmed that we can successfully grow  $\text{In}_x\text{Ga}_{1-x}\text{N}$  films over the entire composition range ( $x=0.16, 0.37-0.47, 0.53, 0.63, 0.68, 0.73, 0.94, 0.97$ ). Phase separation did not occur in  $\text{In}_x\text{Ga}_{1-x}\text{N}$  films with  $x > 0.53$ .<sup>39)</sup> This is probably due to the relatively low growth temperature and the insertion of an InN buffer layer.

Because of the slow atom migration at low temperature, complete equilibrium might not have occurred during growth. In addition, the thermodynamical calculations by Kangawa *et al.*<sup>41)</sup> showed that the mixing enthalpy of InGaN is much smaller on an InN substrate than on a GaN substrate. They reported that the mixing enthalpy of InGaN became even smaller than that of free-standing InGaN when they were grown on InN. These effects can probably explain why we could grow In-

GaN over the entire alloy composition range.

Figures 23 and 24 show the CL and PL spectra obtained at liquid-nitrogen temperature, respectively. CL and PL emissions were observed for all samples, confirming their good crystalline quality.

Figure 25 shows the absorption and PL spectra of 10 samples with different alloy compositions ranging between  $x=0$  and  $x=1.0$ . The luminescence peak position and absorption edge roughly agree for all the samples over the entire alloy composition range. Figure 26 shows peak energies obtained from the CL and PL spectra as functions of In composition. This figure also includes the results reported by other authors.<sup>42-44)</sup> The plots of the luminescence peak positions in Fig.26 can be fit to a smooth curve  $E_0 = 3.48 - 2.70x - bx(1-x)$  with a bowing parameter  $b = 2.3$  eV.<sup>39)</sup> Here, the Moss-Burstein effect is not taken into account.

These results on the optical properties of InGaN over the entire alloy composition range are consistent with the InN bandgap energy of about 0.8 eV.

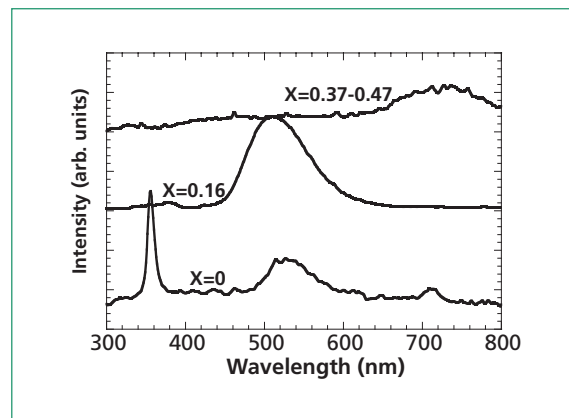


Fig.23. CL spectra at 77 K for the  $\text{In}_x\text{Ga}_{1-x}\text{N}$  samples ( $x=0, 0.16, 0.37-0.47$ ).

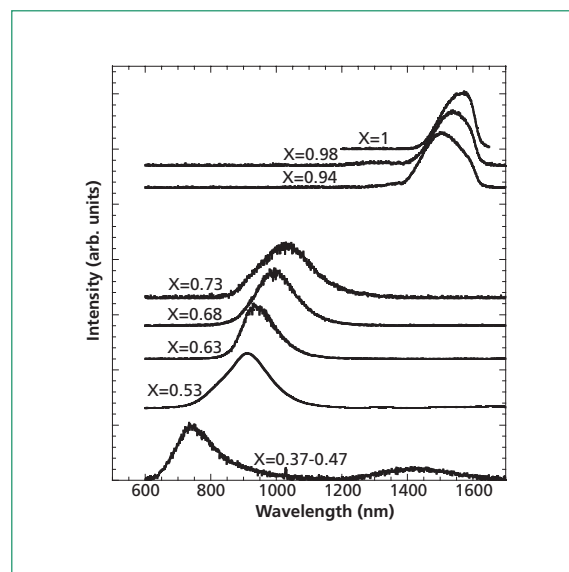


Fig.24. PL spectra at 77 K for the  $\text{In}_x\text{Ga}_{1-x}\text{N}$  samples ( $x=0.37-0.47, 0.53, 0.63, 0.68, 0.73, 0.94, 0.98, 1$ ).

## 6. Conclusions

Recent developments in growth and characterization of InN and related alloys are reviewed. InN and InGaN growth on (0001) sapphire was studied by RF-plasma-excited molecular beam epitaxy. In this growth method, neutral and ionized, excited nitrogen atoms and molecules are generated using a plasma source. Thus, the crystal growth temperature can be set independent of the requirements for pyrolysis of a nitrogen source. This enabled us to grow InN at a relatively low temperature without noticeable dissociation of the InN surface.

It was shown that nitridation of the sapphire substrates prior to growth is very effective for producing single crystals. It was also suggested that an atomically flat surface is essential for obtaining high-quality InN films. The two-step growth method involving low-

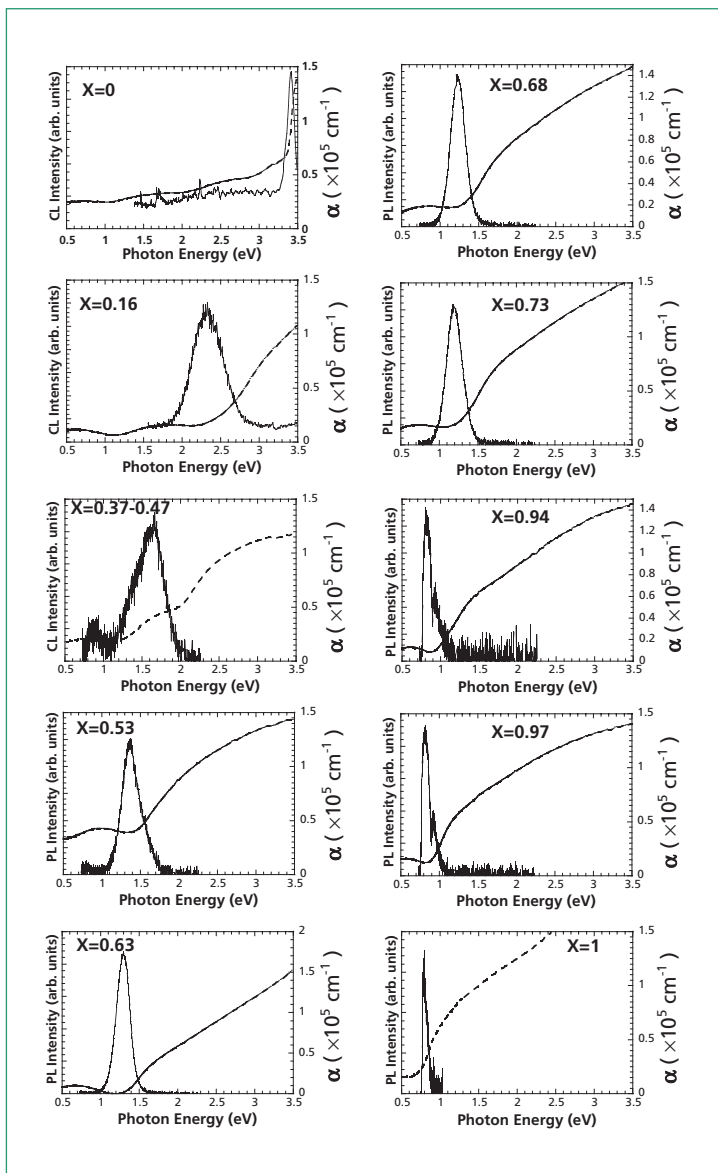


Fig.25. Absorption and PL spectra at room temperature of  $\text{InGa}_{1-x}\text{N}$  samples with different alloy compositions between  $x=0$  and  $x=1.0$ . Dashed line shows CL or PL spectrum. Dotted line shows absorption spectrum.

temperature buffer layer growth at around  $300^\circ\text{C}$  and consecutive annealing at  $550^\circ\text{C}$  was shown to be very effective in obtaining smooth surfaces.

The control of V/III ratio and growth temperature is also extremely important. To obtain high-quality InN films, the growth temperature should be set as high as possible within the dissociation limit of InN. V/III ratio, on the other hand, should be controlled as close as possible to stoichiometry from the N-rich side.

The growth of thick InN without In droplets is very difficult. Once the beam equivalent pressure of In becomes higher than the equivalent nitrogen pressure, In droplets

form which do not evaporate from the surface. This degrades film quality. The insertion of low-temperature intermediate layers was found to be effective in obtaining relatively thick InN. As the crystal quality is poor in and around the low-temperature buffer layer, the overall InN crystal quality improved with increase in InN thickness.

Thick, high-quality InN with an XRC FWHM of  $236.7$  arcsec and  $\omega-2\theta$  XRD FWHM of  $28.9$  arcsec was obtained. As for its electrical properties, a carrier concentration of  $4.9 \times 10^{18} \text{ cm}^{-3}$  and a room temperature mobility of  $1130 \text{ cm}^2/\text{Vs}$  were obtained. Optical absorption and PL were also studied using high-quality InN. A very strong, sharp lumines-

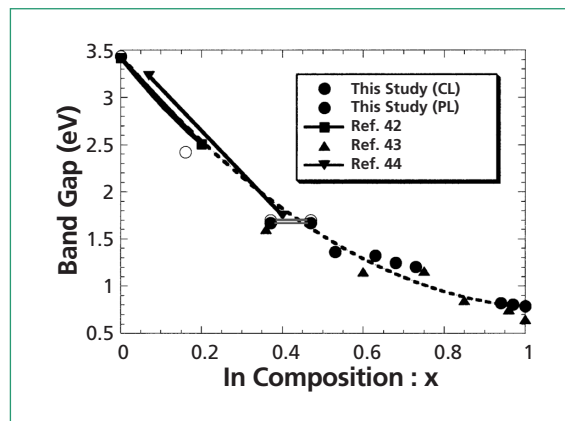


Fig.26. Peak positions of CL and PL spectra at 77 K as functions of In composition. This figure also includes the results reported by other authors.<sup>42-44</sup>

cence was observed both at 77 K and room temperature; the corresponding FWHMs were 24 meV and 38 meV, respectively.

These results obtained by optical measurements suggest that the fundamental band gap of high-quality single-crystalline InN is about 0.8 eV at room temperature.

InGaN films with an entire alloy composition were grown at  $550^\circ\text{C}$  without noticeable phase separation. The plots of the band gaps of these InGaN films against In composition also suggest that InN fundamental band gap should be approximately 0.8 eV.

Thus, this study offers a series of sufficiently convincing results to unequivocally state that the fundamental bandgap of InN is about 0.8 eV rather than long-believed value of 1.9 eV. This finding also suggests that the optical application field of nitride semiconductors covers the range from ultraviolet (6.2 eV) to infrared (0.8 eV), which correspond to the wavelength used for optical communications.

## Acknowledgements

The authors thank M. Hori and K. Kano for MBE growth experiments. Thanks are also due to H. Harima for Raman scattering measurements and T. Miyajima for EXAFS measurements. The author acknowledges the help of J. Wu, W. Walukiewicz in optical characterization, A. Kasic in infrared spectroscopic ellipsometry and S. Pereira in RBS measurements. They also thank T. Araki, N. Teraguchi, A. Suzuki and V. Y. Davydov for fruitful discussions. This work was supported by the Ministry of Education, Culture, Sports, Science and Technology, Grant-in-Aid for Scientific Research (B) #13450131, 2002 and Academic Frontier Promotion Project. **JSAP**

## References

- 1) F. Fischer and F. Schröter: *Ber. Dtsch. Keram. Ges.* **43** (1910) 1465.
- 2) J. B. MacChesney, P. M. Bridenbaugh and P. B. O'Connor: *Mater. Res. Bull.* **5** (1970) 783.
- 3) K. Osamura, S. Nara and Y. Murakami: *J. Appl. Phys.* **46** (1975) 3432.
- 4) H. J. Hovel and J. J. Cuomo: *Appl. Phys. Lett.* **20** (1972) 71.
- 5) K. L. Westra, R. P. W. Lawson and M. J. Brett: *J. Vac. Sci. Technol. A* **6** (1988) 1730.
- 6) K. Osamura, K. Nakajima and Y. Murakami: *Solid State Commun.* **11** (1972) 617.
- 7) J. W. Trainor and K. Rose: *J. Electron. Mater.* **3** (1974) 821.
- 8) N. Puychevriev and M. Menoret: *Thin Solid Films* **36** (1976) 141.
- 9) V. A. Tyagai, A. M. Evstigneev, A. N. Krasiko, A. F. Andreeva and V. Y. Malakhov: *Sov. Phys. Semicond.* **11** (1977) 1257.
- 10) B. R. Natarajan, A. H. Eltoukhy and J. E. Greene: *Thin Solid Films* **69** (1980) 201.
- 11) H. Takeda and T. Hada: *Toyama Kogyo Koto Semmon Gakko Kiyo* **11** (1977) 73 (in Japanese).
- 12) T. L. Tansley and C. P. Foley: *J. Appl. Phys.* **59** (1986) 3241.
- 13) T. Matsuoka, H. Tanaka and A. Katsui: *Int. Symp. on GaAs and Related Compounds, Karuizawa, Japan 1989*, *Inst. Phys. Conf. Ser.* **106** (1990) p.141.
- 14) A. Yamamoto, T. Shinya, T. Sugiura and A. Hashimoto: *J. Cryst. Growth* **189** (1998) 461.
- 15) S. Yamaguchi, M. Kariya, S. Nitta, T. Takeuchi, C. Wetzel, H. Amano and I. Akasaki: *J. Appl. Phys.* **85** (1999) 7682.
- 16) A. Yamamoto, T. Tanaka, K. Koide and A. Hashimoto: *Phys. Status Solidi B* **194** (2002) 510.
- 17) W. E. Hoke, P. J. Lemonias and D. G. Weir: *J. Cryst. Growth* **111** (1991) 1024.
- 18) M. Higashiwaki and T. Matsui: *Jpn. J. Appl. Phys.* **41** (2002) L540.
- 19) H. Lu, W. J. Schaff, J. Hwang, H. Wu, G. Koley and L. F. Eastman: *Appl. Phys. Lett.* **79** (2001) 1489.
- 20) Y. Saito, N. Teraguchi, A. Suzuki, T. Araki and Y. Nanishi: *Jpn. J. Appl. Phys.* **40** (2001) L91.
- 21) T. Inushima, V. V. Mamutin, V. A. Vekshin, S. V. Ivanov, T. Sakon and S. Motokawa: *J. Cryst. Growth* **227** (2001) 481.
- 22) V. Y. Davydov, A. A. Klochikhin, R. P. Seisyan, V. V. Emtsev, S. V. Ivanov, F. Bechstedt, J. Furthmuller, H. Harima, A. V. Mudryi, J. Adrhold, O. Semchinova and J. Graul: *Phys. Status Solidi B* **229** (2002) R1.
- 23) T. Matsuoka, H. Okamoto, M. Nakao, H. Harima and E. Kurimoto: *Appl. Phys. Lett.* **81** (2002) 1246.
- 24) J. Wu, W. Walukiewicz, K. M. Yu, J. W. Arger, III, E. E. Haller, H. Lu, W. J. Schaff, Y. Saito and Y. Nanishi: *Appl. Phys. Lett.* **80** (2002) 3967.
- 25) Y. Saito, H. Harima, E. Kurimoto, T. Yamaguchi, N. Teraguchi, A. Suzuki, T. Araki and Y. Nanishi: *Phys. Status Solidi B* **234** (2002) 796.
- 26) A. Wakahara and A. Yoshida: *Appl. Phys. Lett.* **54** (1989) 709.
- 27) T. Yamaguchi, Y. Saito, K. Kano, T. Araki, N. Teraguchi, A. Suzuki and Y. Nanishi: *Proc. Int. Conf. Indium Phosphide and Related Materials, 2002*, PII-41, p.643.
- 28) T. Yamaguchi, Y. Saito, K. Kano, T. Araki, N. Teraguchi, A. Suzuki and Y. Nanishi: *Phys. Status Solidi B* **228** (2001) 17.
- 29) T. Yamaguchi, T. Araki, Y. Saito, T. Maruyama, Y. Nanishi, N. Teraguchi and A. Suzuki: *Inst. Phys. Conf. Ser.* **170** (2002) 765.
- 30) A. Yamamoto, Y. Murakami, K. Koide, M. Adachi and A. Hashimoto: *Phys. Status Solidi B* **228** (2001) 5.
- 31) Y. Saito, N. Teraguchi, A. Suzuki, T. Araki and Y. Nanishi: *Proc. Int. Workshop Nitride Semiconductors* (The Institute of Pure and Applied Physics, Tokyo, 2000) IPAP Conf. Series 1, p. 182.
- 32) S. V. Ivanov: *Nitride Semiconductors (Handbook on Materials and Devices)*, eds. P. Ruterana, M. Albrecht and J. Neugebauer (Wiley-VCH, Berlin, 2002).
- 33) Y. Saito, N. Teraguchi, A. Suzuki, T. Yamaguchi, T. Araki and Y. Nanishi: *Mat. Res. Symp. Proc.* **639** (2001) G11.18.
- 34) Y. Saito, Y. Tanabe, T. Yamaguchi, N. Teraguchi, A. Suzuki, T. Araki and Y. Nanishi: *Phys. Status Solidi B* **228** (2001) 13.
- 35) M. Mayumi, F. Sato, Y. Kumagai, K. Takemoto and A. Koukitsu: *Phys. Status Solidi B* **228** (2001) 537.
- 36) Y. Saito, T. Yamaguchi, H. Kanazawa, K. Kano, T. Araki, Y. Nanishi, N. Teraguchi and A. Suzuki: *J. Cryst. Growth* **237-239** (2002) 1017.
- 37) T. Miyajima, Y. Kudo, K. L. Liu, T. Uruga, T. Honma, Y. Saito, M. Hori, Y. Nanishi, T. Kobayashi and S. Hirata: *Phys. Status Solidi B* **234** (2002) 801.
- 38) A. Kasic, M. Schubert, Y. Saito, Y. Nanishi and G. Wagner: *Phys. Rev. B* **65** (2002) 115206.
- 39) M. Hori, K. Kano, T. Yamaguchi, Y. Saito, T. Araki, Y. Nanishi, N. Teraguchi and A. Suzuki: *Phys. Status Solidi B* **234** (2002) 750.
- 40) N. Yoshimoto, T. Matsuoka, T. Sasaki and A. Katsui: *Appl. Phys. Lett.* **59** (1991) 2251.
- 41) Y. Kangawa, T. Ito, A. Mori and A. Koukitsu: *J. Cryst. Growth* **220** (2000) 401.
- 42) C. Wetzel, T. Takeuchi, S. Yamaguchi, H. Kato, H. Amano and I. Akasaki: *Appl. Phys. Lett.* **73** (1998) 1994.
- 43) V. Y. Davydov, A. A. Klochikhin, V. V. Emtsev, S. V. Ivanov, V. V. Vekshin, F. Bechstedt, J. Furthmuller, H. Harima, A. V. Mudryi, A. Hashimoto, A. Yamamoto, J. Adrhold, J. Graul and E. E. Haller: *Phys. Status Solidi B* **230** (2002) R4.
- 44) K. P. O'Donnell, J. F. W. Mosselmanns, R. W. Martin, S. Pereira and M. E. White: *J. Phys.: Condens. Matter* **13** (2001) 6977.



Yasushi Nanishi was born in Tokushima Prefecture, Japan in 1945. He received a B.E. degree from Nagoya Institute of Technology in 1969 and M.E. and Ph. D. degrees from Nagoya University in 1971 and 1986, respectively. From 1971 to 1994, he was a member of a

research staff at NTT LSI and Opto-electronics Laboratories, Atsugi, Japan. From 1978 to 1980, he was a visiting scientist at Massachusetts Institute of Technology. Since 1994 he has been a professor in the Department of Photonics at Ritsumeikan University. He has been engaged in the research fields concerning GaAs MES FETs, Liquid Phase Epitaxy of GaAs, growth and characterization of bulk GaAs, correlation between GaAs crystal defects and FET performances and Plasma Excited Molecular Beam Epitaxy. His latest interests are in MBE growth of Nitride Semiconductors and its application to both electronic and optoelectronic devices. He has been a leader of NEDO's regional consortium project and METI's national project on high-power, high-frequency GaN electronic devices. He is a member of The Japan Society of Applied Physics, The Institute of Electrical Engineers of Japan, The Institute of Electronics, Information and Communication Engineers, The Japanese Association for Crystal Growth and American Material Research Society.



Yoshiki Saito was born in Hyogo Prefecture, Japan on April 7, 1975. He received his B.E., M.E. and Ph. D. degrees in Science and Engineering from Ritsumeikan University in 1998, 2000 and 2003, respectively. He is currently belonging to Faculty of Science and Engineering

of Ritsumeikan University. His current research interests are growth and characterization of InN and related alloy semiconductors by RF-Plasma-Excited Molecular Beam Epitaxy. He is a member of The Japan Society of Applied Physics.



Tomohiro Yamaguchi was born in Nagano Prefecture, Japan on March 1, 1978. He received his M.E. degree in Science and Engineering from Ritsumeikan University in 2001. He is currently working toward the Ph. D in the Department of Photonics, Ritsumeikan

University. His current research interests are the initial growth study and characterization of InN and related alloy semiconductors. He is a member of The Japan Society of Applied Physics, The Japanese Association for Crystal Growth and The Institute of Electronics, Information and Communication Engineers.